Quantitative analysis on the mechanism of Cd^{2+} removal by $MgCl_2$-modified biochar in aqueous solutions

Published in: *Journal of Hazardous Materials*

Citation for published version: Yin, G., Tao, L., Chen, X., Bolan, N.S., Sarkar, B., Lin, Q., Wang, H., (2021) Quantitative analysis on the mechanism of Cd^{2+} removal by $MgCl_2$-modified biochar in aqueous solutions. *Journal of Hazardous Materials*. 420: 126487. doi: 10.1016/j.jhazmat.2021.126487.

Document version: Accepted peer-reviewed version.

Quantitative analysis on the mechanism of Cd^{2+} removal by $MgCl_2$-modified biochar in aqueous solutions

Guangcai Yin[a,1], Lin Tao[a,1], Xinglin Chen[a], Nanthi S. Bolan[b], Binoy Sarkar[c], Qintie Lin[a], Hailong Wang[d,e,*]

[a] *Guangdong Industrial Contaminated Site Remediation Technology and Equipment, Engineering Research Center, School of Environmental Science and Engineering, Guangdong University of Technology, Guangzhou, 510006, China*

[b] *The Global Centre for Environmental Remediation, University of Newcastle, Callaghan, NSW, Australia*

[c] *Lancaster Environment Centre, Lancaster University, Lancaster, LA1 4YQ, United Kingdom*

[d] *Biochar Engineering Technology Research Center of Guangdong Province, School of Environmental and Chemical Engineering, Foshan University, Foshan 528000, China*

[e] *Key Laboratory of Soil Contamination Bioremediation of Zhejiang Province, Zhejiang A &F University, Hangzhou 311300, China*

[1] These authors contributed equally to this work and should be considered as co-first authors.

* Correspondence to: School of Environmental and Chemical Engineering, Foshan University, Foshan, Guangdong 528000, China. E-mail address: hailong.wang@fosu.edu.cn.

Graphical abstract

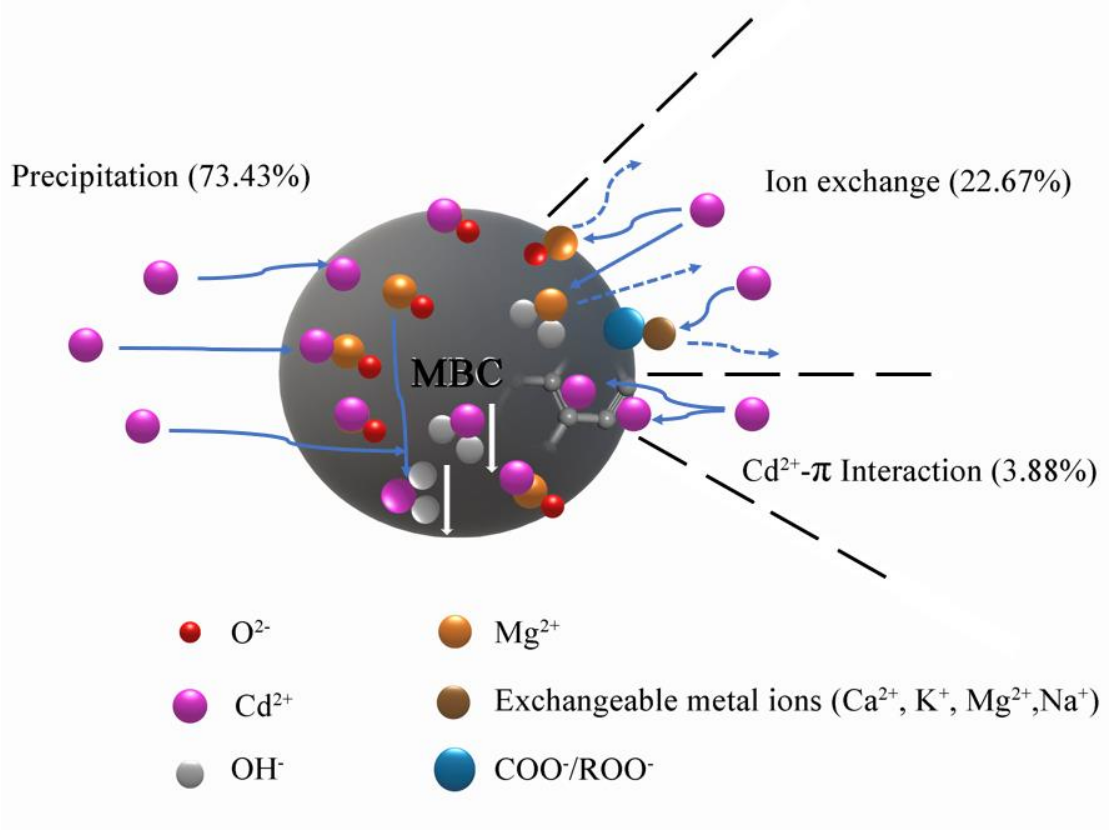

Highlights

- $MgCl_2$ modification increased the specific surface area and pore volume of biochar.
- $MgCl_2$ modified biochar removed 763.12 mg/g Cd^{2+} from polluted water.
- $Cd(OH)_2$ precipitation dominated the Cd^{2+} removal mechanism.

Abstract

In this study, a pristine biochar (BC) and $MgCl_2$-modified biochar (MBC) were prepared using *Pennisetum sp.* straw for removing Cd^{2+} from aqueous solutions. Scanning electron microscope (SEM) imaging combined with energy dispersive X-ray spectroscopy (EDX), X-ray photoelectron spectroscopy (XPS), Fourier transform infrared spectroscopy (FTIR), as well as the surface area and porosity analyses were used to reveal the physico-chemical characteristics of the pristine and modified adsorbents. Results suggested that $MgCl_2$ impregnation during the synthesis had enhanced the specific surface area and pore volume of the biochar. Batch adsorption experiments showed that the Cd^{2+} adsorption data of MBC fitted to the Langmuir isotherm and pseudo-second order kinetic models, indicating a chemical adsorption was undergoing in the system. The maximum adsorption capacity of Cd^{2+} on MBC was 763.12 mg/g, which was 11.15 times higher than that of the pristine BC. The Cd^{2+} removal by MBC was mainly attributed to the mechanisms in an order: $Cd(OH)_2$ precipitation (73.43%) > ion exchange (22.67%) > Cd^{2+}-π interaction (3.88%), with negligible contributions from functional group complexation and physical adsorption. The MBC could thus be used as a promising adsorbent for Cd^{2+} removal from aqueous solutions.

Keywords: Engineered biochar; Cadmium removal; Adsorption; Surface characterization; Wastewater treatment.

1. Introduction

Cadmium (Cd) in wastewater is an environmental concern because the element is non-biodegradable, and poses risks to human health through the food chain and drinking water contamination (Chen et al., 2020; Lian et al., 2020). It is imperative to develop an efficient and cost-effective method to remove Cd^{2+} from wastewater. A number of methods including precipitation, adsorption, and membrane filtration can be used for Cd^{2+} removal from wastewater (Purkayastha et al., 2014; Xiong et al., 2015), among which adsorption is believed to be an extensively applied method, due to the comparatively easier manipulation, extensive material sources, high efficiency, and low cost of operation (Yoon et al., 2017). Studies have shown that carbonaceous materials, such as activated carbon (Kim et al., 2020), graphene (Zong et al., 2020; Fang et al., 2020), chitosan (Małgorzata et al., 2020), and metallic oxides such as magnetite (Hong et al., 2020) could adsorb Cd^{2+} from aqueous solutions. However, application of the above adsorbents in sewage and wastewater treatment plants was limited owing to the complicated preparation process of the adsorbents, their low adsorption efficiency, and high capital investment (Liu et al., 2020).

Biochar has been favored as a new adsorbent, attributed to its large specific surface area (S_{BET}), high pH, abundant charges on the surface, high porosity, and plentiful of oxygen-containing functional groups (Bandara et al., 2019; Kwon et al., 2020). Various studies have demonstrated that the Cd^{2+} adsorption capacity in the aqueous solution can be enhanced via biochar modification (Nie et al., 2021; Shaheen et al., 2019; Wen et al., 2021). Studies have shown that biochar being chemically modified by magnesium (Mg) ions or compounds (i.e., $MgCl_2$, MgO) can effectively increase the S_{BET} and O/C ratio, thus enhance the Cd^{2+} adsorption capacity. For example, Tao et al. (2019) modified *Thalia dealbata* biochar with $MgCl_2$, which increased S_{BET} of the modified biochar to 110.6 m^2/g, about 15.6 times higher than that of the pristine biochar. The O/C ratio of $MgCl_2$-modified *Thalia dealbata* biochar increased from 0.16 to 0.28, indicating that the number of organic functional groups increased significantly, and the maximum adsorption capacity of Cd^{2+} was approximately 1.5 times higher than that of the pristine biochar. Similar conclusions were also confirmed by Zhang et al. (2021). However, Hou (2017) found that the S_{BET} of $MgCl_2$-modified cow manure biochar was decreased from 2.23, 3.82, and 12.23 m^2/g before modification to 0.33, 2.05, and 6.92 m^2/g after modification when pyrolyzed at 300 ℃, 450 ℃ and 600 ℃. Therefore, uncertainties

still exist on the effect of $MgCl_2$ modification of biochar for Cd^{2+} adsorption. Li et al. (2020) modified four types of straws (corn, taro, cassava, and banana) and one type of shell (camellia nut) biochar with $MgCl_2$. In their studies, the maximum theoretical Cd^{2+} adsorption capacity was 66.23, 96.15, 185.19, 238.10, and 333.33 mg/g, respectively (Li et al., 2020). When studying MgO-modified biochar, Xiang et al. (2018a) modified rice husk biochar with MgO, raising the S_{BET} from 4.23 to 20.64 m^2/g, and subsequently the amount of Cd^{2+} adsorption (18.10 mg/g) was 2.85 times enhanced than that of the pristine biochar. The advantage of $MgCl_2$ modification in solution impregnation was that the pretreatment intensively dehydrated and carbonized the straw biochar, and formed open pores under heating conditions (≥ 500 ℃) (Li et al., 2016). Considering the highly efficient Cd^{2+} adsorption performances, we deduced that $MgCl_2$-modified straw biochar could be an ideal adsorbent for treating Cd-contaminated wastewater, but the mechanism for the enhanced Cd^{2+} adsorption due to $MgCl_2$ modification of biochar is still unclear.

In our previous study, three kinds of *Pennisetum sp*. straw biochar (modified with H_2O_2, $KMnO_4$, and $Fe(NO_3)_3$) were prepared with relatively small S_{BET} of 3.13, 4.70 and 8.80 m^2/g, respectively (Yin et al., 2019; 2020). In this study, we modified the *Pennisetum sp*. straw biochar with $MgCl_2$, aiming at: (1) altering the S_{BET} of the modified biochar (MBC), and (2) quantifying the contributions of Cd^{2+} removal mechanisms, including mineral precipitation, ion exchange, functional group complexation, physical adsorption, electrostatic attraction, and Cd^{2+}-π interactions, from aqueous solutions by MBC.

2. Materials and methods

2.1 Chemicals

Cadmium nitrate ($Cd(NO_3)_2$, analytical reagent (AR) grade), anhydrous magnesium chloride ($MgCl_2$, AR), and sodium nitrate ($NaNO_3$, AR) were procured from Guangzhou Chemical Reagent Factory. Ultrapure water was obtained using a laboratory water purification unit (Clever-S15, Zhiang Instrument Co., Ltd, Shanghai).

2.2 Preparation of biochar

The *Pennisetum sp*. straw, a weed species, was collected from a farmland in Guangzhou City, Guangdong Province, China. The straw was rinsed with ultra-pure water, dried at 60 ℃ to constant weight, cut into 3-4 cm pieces, ground, and passed through a 100-mesh sieve.

The ground *Pennisetum sp*. straw (20 g) was pyrolyzed in a tube furnace with nitrogen (N_2) as the inert gas (200 mL/min), and the temperature was raised up to 500 °C gradually at the rate of 5 °C/min, with the final temperature lasting for 2 h, and then stored in a desiccator.

$MgCl_2$-modified biochar (MBC) was prepared by soaking 10 g *Pennisetum sp*. straw powder to a $MgCl_2$ (1 mol/L, 100 mL) solution, magnetically stirred the mixture for 0.5 h, and dried at 60 °C before the pyrolysis. The composite material was pyrolyzed as above, and stored in a desiccator.

To conduct physicochemical characterization, Cd^{2+}-loaded biochar (BC-Cd) and Cd^{2+}-loaded modified biochar (MBC-Cd) were obtained by mixing 0.025 g BC and MBC sample with 25 mL Cd^{2+} solutions (100 and 1000 mg/L in the case of BC and MBC, respectively), and shaken on a water bath thermostat at 25 ℃ with 200 rpm for 24 h. The mixture was filtered through double circle qualitative filter paper (diameter = 15 ± 0.02 cm), and the solid was dried at 60 °C to obtain BC-Cd and MBC-Cd. Triplicate samples were prepared for the analyses.

2.3 Biochar characterization

An elemental analyzer (Euro VectorEA3000, Italy) was used for determining the total carbon, hydrogen, oxygen, nitrogen, and sulfur contents of the biochar samples. Using KBr as the matrix, the infrared spectra of both the pristine and modified biochars were recorded within the spectral range of 4000-400 cm^{-1} (Is50R, Thermo Fisher, USA). A surface area and porosity analyzer (ASAP 2460, Micromeritics, USA) was used to determine the S_{BET}, and average pore diameter at 77 K. The elemental valence state on the surface of the adsorbents was analyzed by X-ray photoelectron spectroscopy (XPS, Escalab 250 xi, Thermo Fisher, USA), and the scanning range was 10° - 80° at 2θ, with a rotation rate of 2 r/s. The morphology of biochars was observed by a scanning electron microscope equipped with an energy dispersive spectrometer (SEM-EDX, TM3030, Hitach, Japan) to determine the elemental contents. The crystal structures of both the biochars were determined using an X-ray diffractometer (XRD, Ultima III, Japan).

2.4 Batch adsorption experiment

Solutions with different concentrations of Cd^{2+} were prepared by dissolving AR grade $Cd(NO_3)_2$ in ultra-pure water. NaOH (0.05 mol/L) and HNO_3 (0.05 mol/L) were used judiciously to adjust the pH value of the solutions when needed. The pH value of the solution was measured with a laboratory pH meter (STARTCR3100, OHAUS,

USA).

In the adsorption kinetic experiments, 5000 mg/L Cd^{2+} stock solution was used to prepare 100 and 1000 mg/L working solutions. Biochar sample (0.025 g) was placed in a 50 mL polyethylene centrifuge tube, and 25 mL solution with different Cd^{2+} concentrations was added into it. The pH value was adjusted to 5.00±0.05, and the sample was mixed by stirring on a water bath thermostat at 25 °C with 200 rpm. Sub-samples were collected at 5, 10, 30, 60, 90, 120, 240, 480, 600, 960, and 1440 min, and filtered through a 0.45 μm water-based microporous membrane. The filtrate was measured by flame atomic adsorption spectrometer (FAAS) (Z2000, Hitach, Japan). Pseudo-first and pseudo-second order kinetic equations were used to fit the adsorption kinetic data using the OriginPro 2021 software package.

In the adsorption isotherm experiments, 5000 mg/L Cd^{2+} stock solution was used to prepare 20, 40, 60, 80, 100, 120, 160, 180, 200, 400, 600, 800, 1000, 1200, 1500 mg/L initial adsorbate concentration solutions, and the pH was adjusted to 5.00±0.05. A 0.025 g sample of biochar was added into a 50 mL polyethylene centrifuge tube with 25 mL of Cd^{2+} solution at different concentrations, and shaken on a water bath thermostat at 25 ℃, 35 ℃, and 45 ℃ at 200 rpm for 24 h. The suspension was filtered through a 0.45 μm aqueous microporous membrane, and the Cd^{2+} content in the filtrate was measured by FAAS as described above. The adsorption data were fitted to the Langmuir and Freundlich isothermal equations. The adsorbed amount of Cd^{2+} was calculated according to Eq. 1:

$$q_e = \frac{(C_0 - C_e)\cdot V}{W} \quad (1)$$

where, q_e (mg/g) is the adsorption concentrations of Cd^{2+} at equilibrium, V (L) is the volume of Cd^{2+} solution, W (g) is the mass of the biochar, and C_0 and C_e (mg/L) are the initial and equilibrium concentrations of Cd^{2+} in the solution.

The data quality in this study was checked through the analysis of a certified standard of multi-metal solution, standard curve preparation, and parallel standard sample analysis. The standard curves were established with correlation coefficients between 0.9996 and 0.9999.

2.5 Quantitative analysis of different mechanisms of Cd^{2+} adsorption

To undertake an impregnation demineralization of the biochar samples, 10 g of BC or MBC was added to 150 mL of 1 mol/L HCl, stirred continuously for 24 h on a magnetic stirrer at 100 rpm, and then centrifuged at 4000 rpm for 20 min. The solid

products were rinsed with ultra-pure water until the pH value of the leachate remained unchanged. Finally, the solid was dried at 60 °C for 24 h to obtain the demineralized biochar (BCA and MBCA respectively obtained from BC and MBC). Most minerals in biochar were removed by 1 mol/L HCl, and the oxygen-containing functional groups on the surface remained unchanged (Zhang et al., 2017a).

I. Mineral precipitation (Q_{cmp}): The adsorption mechanisms of Cd^{2+} on biochar minerals could include ion exchange (Q_{cme}) and mineral precipitation (Q_{cmp}) (Cui et al., 2016). To elucidate the above, a 0.025 g sample of BCA or MBCA was added into a 50 mL polyethylene centrifuge tube with 25 mL of Cd^{2+} (100 mg/L for BCA, or 1000 mg/L for MBCA) solution, and shaken on a water bath thermostat at 25 ℃ at 200 rpm for 24 h. Each sample was replicated three times. The mixture was filtered through a 0.45 μm aqueous microporous membrane, and the Cd^{2+} content was measured by FAAS, as described above. The amounts of Cd^{2+} adsorbed through mineral precipitation and ion exchange were calculated by Eq. 2 and 3:

$$Q_{cm} = Q_t - Q_a \quad (2)$$

$$Q_{cmp} = Q_{cm} - Q_{cme} \quad (3)$$

where, Q_t (mg/g) is the total amount of Cd^{2+} adsorbed by BC or MBC; Q_a (mg/g) is the total amount Cd^{2+} adsorbed by BCA or MBCA, Q_{cm} (mg/g) is the amount of Cd^{2+} adsorbed by BC or MBC through ion exchange and mineral precipitation, Q_{cmp} (mg/g) is the amount of Cd^{2+} adsorbed by BC or MBC through mineral precipitation, and Q_{cme} (mg/g) is the amount of Cd^{2+} adsorbed by BC or MBC through ion exchange.

II. Ion exchange (Q_{cme}): The difference between the concentration of cations (K^+, Ca^{2+}, Na^+, Mg^{2+}) in the solution before and after Cd^{2+} adsorption was the exchangeable metal cations of biochar (Wu et al., 2019). To evaluate the contribution of adsorption by ion exchange, a 0.025 g sample of BC or MBC was mixed with 25 mL of Cd^{2+} (100 mg/L for BC or 1000 mg/L for MBC) solution, and shaken on a water bath thermostat at 25 ℃ with for 24 h at 200 rpm. Each sample was replicated three times. The sample was filtered through a 0.45 μm aqueous microporous membrane, and the K^+, Ca^{2+}, Na^+, Mg^{2+} content in the filtrate before and after Cd^{2+} adsorption by biochar was measured by ion chromatography (Eco, Metrohm AG, Switzerland). The amount of Cd^{2+} adsorbed by cation exchange was calculated using Eq. 4:

$$Q_{cme} = Q_K + Q_{Ca} + Q_{Na} + Q_{Mg} \quad (4)$$

where, Q_k (mg/g), Q_{Ca} (mg/g), Q_{Na} (mg/g) and Q_{Mg} (mg/g) are the quantities of

Cd^{2+} exchanged with K^+, Ca^{2+}, Na^+ and Mg^{2+}, respectively.

III. Oxygen-containing functional group complexation (Q_{co}): The -COOH and -OH groups of biochar would release H^+ through ion exchange, causing a change of pH value (Cao et al., 2009), which could be described by Eq. 5 and 6. The content of Cd^{2+} adsorbed by oxygen-containing functional groups (Q_{co}) (mg/g) could be calculated by taking the decrease in pH value before and after adsorption of Cd^{2+} by the BC or MBC as the index of H^+ release.

$$-COOH + Cd^{2+} + H_2O \rightarrow -COOCd^+ + H_3O^+ \quad (5)$$

$$-OH + Cd^{2+} + H_2O \rightarrow -OCd^+ + H_3O^+ \quad (6)$$

IV. Cd^{2+}-π interaction ($Q_{c\pi}$): The Cd^{2+} adsorption mechanisms of BCA/MBCA were expected to be through oxygen-containing functional group complexation (Q_{co}) (mg/g) and Cd^{2+}-π interaction ($Q_{c\pi}$) (mg/g), which could be deduced using Eq. 7:

$$Q_{c\pi} = Q_a - Q_{co} \quad (7)$$

V. Physical adsorption (Q_p) and electrostatic attraction (Q_e): The desorption of Cd^{2+} adsorbed by the biochar through Q_p and Q_e could be achieved using 0.01 mol/L $NaNO_3$, and Cd^{2+} adsorbed on biochar through Q_p could be resolved by aqueous solution extraction (Zhang et al., 2020b). In this study, the Cd^{2+} adsorbed by BC or MBC was extracted for 24 h in 0.01 mol/L $NaNO_3$ solution, and then determined the content of Cd^{2+} in the solution. The amounts of Cd^{2+} adsorbed via physical adsorption and electrostatic attraction were calculated using Eq. 8, 9 and 10:

$$Q_{pe} = \frac{C_e \cdot V}{m} \quad (8)$$

$$Q_p = \frac{C_e \cdot V}{m} \quad (9)$$

$$Q_e = Q_{pe} - Q_p \quad (10)$$

where, Q_{pe} (mg/g), Q_p (mg/g), and Q_e (mg/g) are the Cd^{2+} adsorption capacity of BC or MBC through physical adsorption and electrostatic attraction together, only physical adsorption, and only electrostatic attraction, respectively. And, m is the mass of Cd^{2+} (g) adsorbed by BC or MBC.

The relative contribution of different mechanisms to Cd^{2+} adsorption in aqueous solution by BC or MBC were Q_{cmp}/Q_t, Q_{cme}/Q_t, Q_{co}/Q_t, $Q_{c\pi}/Q_t$, Q_p/Q_t, Q_e/Q_t. An average result of three replicates was reported in each case.

3. Results and discussion

3.1 Characterization of BC and MBC

The physical and chemical properties of BC/MBC are listed in Table 1. The C content of MBC decreased by 11.63%, while the O content increased by 10.4%, compared with BC, which were mainly due to the accumulation of a large amount of MgO (17%, Wt%) on MBC. The (O+N)/C, O/C and H/C ratios of MBC increased by 0.21, 0.25 and 0.25 units compared with BC (Table 1), indicating that MBC had a greater proportion of aromatic structures and smaller hydrophilic surface compared with that of BC (Ennis et al., 2012).

SEM images showed that BC (Fig. 1a and Fig. S1a) had a greater proportion of macropores (8.94 nm), and smoother surface than that of MBC (Fig. 1b). Bright materials with high electron yield and abundant small pores on the MBC surface could be observed (Fig. S1b), which might be due to the intense dehydration and carbonization of the biomass during the immersion in $MgCl_2$ solution, followed by pore openings during the pyrolysis (Li et al., 2016). Another reason might be that the $MgCl_2$ impregnation had accelerated the release of volatile substances and formed open pores under heating conditions (Ling et al., 2017). The EDX analysis (Fig.1b) showed that the bright substances deposited on the surface of MBC were formed by Mg and O, as also supported by a previous report where the authors confirmed the bright substances to be MgO (Yin et al., 2018a).

Fig. S2 and Fig. S3 explained the N_2 adsorption–desorption isotherms and pore size distribution of BC/MBC. The isotherms exhibited a typical Langmuir type-IV isotherm with an H_3 hysteresis loop, indicating that mesopores existed in the biochars (Kuang et al., 2019). The average pore diameters of BC and MBC were 8.94 and 3.33 nm (Table 1), and S_{BET} of MBC (202.75 m^2/g) was approximately 107 times higher than that of BC (1.90 m^2/g) (Zhang et al., 2020). The average diameter of MgO particles on the MBC surface was 30.1 nm, as measured by Image J software, which was in line with the result of Yin et al. (2018a), indicating MgO (32.1 nm) nanoparticle formation.

Our results also showed that MBC had a larger pore volume (0.1689 cm^3/g) compared with BC (0.0042 cm^3/g) (Table 1), which might be due to the fact that MgO on the MBC surface had acted as an activator during the pyrolysis (Zhang et al., 2012). However, MBC had a smaller pore diameter (3.33 nm) compared with BC (8.94 nm), indicating the possibility that Mg compounds might have entered and blocked the pores

(Chen et al., 2018).

FTIR was applied to analyze the surface functional groups associated with Cd^{2+} adsorption on BC/MBC (Fig. 2). The band at 3426 cm^{-1} was produced by the stretching vibration of water molecules or phenolic hydroxyl groups. The tensile vibration of Mg-O appeared as a band near 430 cm^{-1}, indicating that MgO was loaded on the BC after $MgCl_2$ impregnation (Jin et al., 2016), which was also confirmed by the EDX data (Fig. 1). The absorption band of $-CH_2$ appeared at approximately 2920 cm^{-1} (Chang et al., 2019), and the tensile vibration of C=C was near 1615 cm^{-1} (Yin et al., 2018b). The absorption band at 1386 cm^{-1} was generated by the C=O symmetric stretching vibration of the carboxyl groups (Qiu et al., 2019), while the band at 1108 cm^{-1} was generated by the C-O stretching vibration of the ether and -COOH groups (Wei et al., 2019). The band at 3450 cm^{-1} shifted to 3426 cm^{-1}, while the 1387 and 1108 cm^{-1} bands shifted slightly to 1386 cm^{-1}/1107 cm^{-1}, and the intensity of 1635 cm^{-1} band significantly decreased (Fig. 2). The above band shifts suggested that $MgCl_2$ impregnation changed the configuration of oxygen-containing functional groups in MBC (Takaya et al., 2016).

The XPS study characterized the electronic structure of BC/MBC. The photoelectron spectra of C1s, O1s, and Mg2p were shown in Fig. 3. The C1s peaked at 284.81, 285.62, 286.7 and 289.57 eV for the BC, and at 284.84, 285.65, 286.86 and 289.4 eV for MBC (Fig. 3a), representing C-C, C-O, C=O and -COOR groups respectively (Miaet al., 2017), which were also confirmed by the IR results (Fig. 2). After modification, the relative content of the C-C group increased by 6.33%, while the total proportion of C=O, C-O and -COOR group contents decreased from 54.38% to 48.05%. Therefore, the $MgCl_2$-modified biochar was able to minimize the oxidation of C-C to oxygen-containing functional groups, which was agreed with the results of Chen et al. (2018). The O1s of BC was deconvoluted into four peaks (Fig. 3b) which were attributed to hydroxyl-bonded metal (M-OH, 530.10 eV), metal oxide (C-OH, 531.37 eV), surface hydroxyl (M-O, 532.42 eV), and adsorbed H_2O (533.25 eV) (Li et al., 2020). At the same time, the relative content of M-OH was significantly reduced by 40.53%, while the ratio of C-OH was raised by 42.21%. The XPS spectrum of Mg2p (Fig. 3c) showed that the Mg peak (50.72 eV) on MBC was MgO (Liu et al., 2013), indicating MgO was successfully introduced into BC.

XRD analysis showed that the main reflection in the pattern of BC was due to KCl (Fig. 4), and several new reflections in MBC were of MgO (JCPDS card number: 84-0653), which again confirmed that Mg had been successfully loaded on BC, and that

MgO was the most important crystal phase (Liu et al., 2013).

3.2 Adsorption kinetics

The Cd^{2+} adsorption data of both the biochars were fitted to the pseudo-first order (PFOM) (Eq. 11) and pseudo-second order (PSOM) kinetic models (Eq. 12) (Fig. S4). The empirical expressions of the two models are Eq. 11 and 12 (Ho et al., 1998).

$$\text{Pseudo-first order model: } \ln\left(1-\frac{q_t}{q_e}\right) = -k_1 \cdot t \quad (11)$$

$$\text{Pseudo-second order model: } \frac{t}{q_t} = \frac{1}{k_2 \cdot q_e^2} + \frac{t}{q_e} \quad (12)$$

where, q_e (mg/L) is the equilibrium concentration of Cd^{2+}, q_t (mg/g) represents the adsorption capacity of Cd^{2+} at time t (min), k_1 (min^{-1}) is the rate constant of the pseudo-first order model, and k_2 (g/(mg/min)) represents the rate constant of pseudo-second order model.

The parameters of the two kinetic models are listed in Table 2. The adsorption capacity of Cd^{2+} on BC/MBC increased with time (0-1440 min), and stabilized after reaching the equilibrium. The adsorption capacities of Cd^{2+} at 240 and 600 min for BC and MBC were close to the saturation (Fig. S4). The adsorption process showed two phases: a fast adsorption in the first 480 min, followed by a significantly slow stage until reaching the equilibrium. The initial rapid stage was due to the numerous adsorption sites present on the biochar, accompanied with a high concentration of Cd^{2+} in the solution (Wan et al., 2020). After that, Cd^{2+} quickly occupied the accessible external adsorption sites (Lian et al., 2015). The slow adsorption stage was due to the diffusion of Cd^{2+} to the carbon pores and interaction with active sites therein over time (Li et al., 2017). Another probable reason was that the movement of Cd^{2+} through the internal pores of biochar was limited (Zhang et al., 2017b). The coefficient of determination (R^2) values of the pseudo-first order and pseudo-second order models for BC were both 0.9999, and those of MBC were 0.9989 and 0.9990, respectively. The relative percent deviation (RPD) values of the pseudo-first order and pseudo-second order models for BC were 4.75 and 49.64, and those of MBC were 3.90 and 92.34, respectively. Therefore, the Cd^{2+} adsorption process on both the biochars fitted better to the pseudo-second order model than the pseudo-first order model, demonstrating that chemical adsorption was the main mechanism in the system (Yin et al., 2020; Liu et al., 2020).

3.3 Adsorption isotherms

The adsorption isotherm parameters are listed in Table 3. The Langmuir and Freundlich models were used to evaluate the effects of Cd^{2+} concentrations (0-2000 mg/L) on Cd^{2+} adsorption by BC and MBC (Fig. 5). The isothermal models are expressed as (Eq. 13-14), and the thermodynamic parameters of adsorption (involving Gibbs free energy ΔG^{o}, entropy ΔS^{o}, and enthalpy ΔH^{o}) are expressed as (Eq. 15-16) (Sarkar et al., 2012).

$$\text{Langmuir model: } q_e = \frac{q_m \cdot K_L \cdot C_e}{1 + K_L \cdot C_e} \quad (13)$$

$$\text{Freundlich model: } q_e = K_F \cdot C_e^{\frac{1}{n}} \quad (14)$$

$$\ln K_c = \frac{\Delta S^\circ}{R} - \frac{\Delta H^\circ}{RT} \quad (15)$$

$$\Delta G^\circ = \Delta H^\circ - T\Delta S^\circ \quad (16)$$

where, q_m (mg/g) is the maximum adsorption capacity, K_L (L/mg) is the Langmuir constant, and K_F ((mg/g) $(L/mg)^{1/n}$) is the Freundlich constant. 1/n is the adsorption strength, which decides the nonlinear degree of adsorption isotherms. R is the universal gas constant (8.314 J/(mol·K)), and T is the absolute temperature (K). K_c represents the adsorption equilibrium constant.

For the Langmuir and Freundlich isotherm model fitting in the case of MBC, the R^2 values were 0.9809 and 0.9417, and the RPD values were 314.29 and 7.12, respectively, which showed that the Cd^{2+} adsorption data fit the Langmuir model better than Freundlich model for MBC. The Langmuir model fitting of the adsorption data suggested that the Cd^{2+} adsorption by MBC was mainly through homogeneous active sites on the surface (Yao et al., 2011). For the isotherm models of BC, the R^2 values were 0.9940 and 0.9618, and the RPD values were 52.69 and 16.07, respectively, which showed that the Cd^{2+} adsorption on BC also fit the Langmuir model better than Freundlich model. The maximum Cd^{2+} adsorption capacity of MBC was 763.12 mg/g, which was approximately 11.15 times higher than that of BC. In addition, MBC had a higher adsorption capacity than most of the formerly reported adsorbents, such as $MgCl_2$-modified coconut shell biochar (77.26 mg/g) (Chen et al., 2020), and MgO-modified rice husk biochar (18.10 mg/g) (Xiang et al., 2018b). The 1/n value for MBC (0.2122) was < 1, again indicating that chemical adsorption took place in the system of MBC (Li et al., 2014).

In the temperature range of 25 ℃ - 45 ℃, all the ΔG^{o} values during the adsorption

of Cd^{2+} on biochars were negative (-9.04 kJ/mol to -1.81 kJ/mol), indicating that the adsorption process was spontaneous (Sarkar et al., 2012). The ΔH^o of BC was negative, which indicated that the process was partially contributed by physical adsorption (Wu et al., 2001). The thermodynamic parameters of MBC were: ΔH^o (8.9 kJ/mol) > 0, ΔS^o (35.93 kJ/mol) > 0, $\Delta G^o < 0$ (Table S1), indicating that the adsorption process was endothermic and spontaneous (Khan et al., 2020).

4. Mechanisms of Cd^{2+} adsorption on biochars

After Cd^{2+} was adsorbed by BC and MBC, the pH value of the solution was 6.53 and 6.14, respectively, and the main Cd species in the aqueous solution was Cd^{2+} (Fig. S5), indicating that the high Cd^{2+} binding was mainly due to the adsorption capacity of the biochars, rather than a precipitation which might otherwise be caused by an alkaline pH value of the solution. As shown in Table 4, the values of Q_p/Q_t, Q_e/Q_t, and Q_{co}/Q_t of BC were 0.31%, 0.38%, and 0.03%, respectively. The Q_p/Q_t, Q_e/Q_t, and Q_{co}/Q_t values of MBC were all less than 0.01%, which suggested that the relative contribution of oxygen-containing functional group complexation, electrostatic attraction and physical adsorption could be neglected. As a result, the mechanisms of Cd^{2+} adsorption by BC or MBC were mainly mineral precipitation, ion exchange, and Cd^{2+}-π interaction. The contribution of various mechanisms to Cd^{2+} removal by biochar followed the order of $Q_{cmp} > Q_{cme} > Q_{c\pi}$, which was consistent with the finding of Cui et al. (2016).

4.1 Mineral precipitation

The contribution of mineral precipitation to Cd removal by MBC (73.43%) was much higher than that of BC (56.28%), where mineral precipitation had contributed the most portion of Cd^{2+} adsorption (Table 4). This might be because MBC had a higher ash content than that of BC (Table 1) (Wang et al., 2018).

After Cd^{2+} was adsorbed by BC and MBC, the O1s photoelectron spectra indicated that the proportion of M-O increased by 23.56% and 17.80% respectively, confirming that Cd-O was formed on biochar surfaces (Zhang et al., 2017a). This was also proved by the photoelectron spectra of Cd3d (Fig. 3d). After Cd^{2+} adsorption on BC, the quantity of C=O and C-O decreased by 10.01% and 7.10%, respectively. After Cd^{2+} adsorption on MBC, the proportion of C=O increased from 11.29% to 21.69%, while that of C-O decreased from 30.67% to 25.31% (Fig. 3a), which agreed with the results of Wang et al. (2018). The XRD patterns showed new crystal phase formation on BC-Cd, demonstrating that $CdCO_3$ (JCPDS card number: 42-1342) was the main

precipitation formed (Liu et al., 2013). The most dominant crystal phase on the surface of MBC-Cd was $Cd(OH)_2$ (JCPDS card number: 84-1767), which was consistent to the finding of Zhu & Li (2012) who found that MgO on the surface of MBC promoted the precipitation of $Cd(OH)_2$.

Previous studies showed that alkaline MgO could be easily hydroxylated in neutral aqueous solution (Xiang et al., 2018b). Once the adsorbent was in contact with MgO, the surface of the MBC might have been hydroxylated (Eq. 17) (Tian et al., 2017). Meanwhile, quite a lot of MgO on MBC could form $Mg(OH)^+$ in the presence of H^+ under acidic conditions (Eq. 18) (Ling et al., 2017). MBC likely adsorbed Cd^{2+} through MgO on the surface forming $Cd(OH)_2$ precipitation (Eq.19) (Xiang et al., 2018b).

$$MgO(s) + H_2O(l) \rightarrow Mg(OH)^+(surface) + OH^- \rightarrow Mg^{2+} + 2OH^- \quad (17)$$

$$MgO(s) + H^+ \rightarrow Mg(OH)^+(surface) \quad (18)$$

$$MgO(s) + H_2O(l) + Cd^{2+} \rightarrow Cd(OH)_2 + Mg^{2+} \quad (19)$$

4.2 Ion exchange

During Cd^{2+} adsorption by MBC, Na^+, Mg^{2+} and K^+ were released into the solution (Fig. S6). The adsorbent surface formed -COOCd and -O-Cd that likely released Mg^{2+} and Ca^{2+}, where K^+ and Na^+ possibly formed outer-sphere complexes in the solution after the ion exchange reaction with Cd^{2+} (Lu et al., 2012). The net concentration of K^+ in BC (10.81 mg/L) was higher than that of MBC (2.44 mg/L). On the contrary, the Mg^{2+} content of MBC (126.76 mg/L) was about 2817 times higher than that of BC (0.045 mg/L), as confirmed by the EDX results. The exchangeable metal cations (e.g., Ca^{2+}, Mg^{2+}, K^+) were retained on the surface of biochar through electrostatic attraction on -COOH or -OH groups, and then exchanged with Cd^{2+} during the adsorption process (Deng et al., 2018). The S_{BET} of biochar was greatly raised by $MgCl_2$ modification, which might have promoted the above ion exchange reaction (Zhang et al., 2020a). Exchangeable metal cations (e.g., Ca^{2+}, Mg^{2+}, K^+) were released into the solutions while Cd^{2+} was being adsorbed. Compared to the BC, the Q_{cme} of MBC for Cd^{2+} increased from 22.9 to 173.0 mg/g (Table 4). These results showed that $MgCl_2$ impregnation significantly improved the ion exchange capacity of biochar, which could also be due to the fact that MgO was successfully loaded on BC (Wu et al., 2021). The ion exchange reactions promoted by MgO could be expressed as Eq. 20 and 21 (Kuang et al., 2019).

$$MgO + H_2O \rightarrow Mg(OH)_2 \quad (20)$$

$$MgO/Mg(OH)_2 + Cd^{2+} \rightarrow CdO/Cd(OH)_2 + Mg^{2+} \quad (21)$$

4.3 Cd^{2+}–π interactions

The $Q_{c\pi}$ of BC and MBC were 6.51 and 29.63 mg/g, respectively (Table 4), indicating that the $MgCl_2$ modification increased the Cd^{2+}-π interaction of biochar during Cd^{2+} adsorption. The EDX results showed that the O content (Wt %) of MBC increased by 6.33% compared to BC, and the binding energy of O1s also increased (Fig. S7). It was reasonable to form Cd^{2+} complexes through π bonding on C=O groups of the biochar (Zhu et al., 2020), because Cd^{2+} would tend to form soft-soft acid-base bonds. This might be due to the aromatic structure of biochar surfaces formed during the high temperature pyrolysis (≥ 500 °C), rendering π donations during Cd^{2+} adsorption (Harvey et al., 2011). The binding energy (405.8 eV) of BC might be related to the Cd^{2+}-π interaction, indicating that Cd^{2+} bonded to the graphene-like aromatic structures of the biochar (Wang et al., 2018). The peak width of C=C (π electrons) increased after Cd^{2+} adsorption, and the binding energy of O1s on biochar increased slightly (Fig. S7), demonstrating that the O atom participated in the Cd^{2+} adsorption process (Zhang et al., 2017a). These results were ascribed to the high degree of graphitization in high-temperature biochar, which enhanced the π donating properties (Xie et al., 2014). The effects of Cd^{2+}-π interactions ($Q_{c\pi}$) on Cd^{2+} adsorption could be expressed as Eq. 22 and 23 (Li et al., 2020).

$$C\pi + 2H_2O \rightarrow C\pi\text{-}H_3O^+ + OH^- \quad (22)$$

$$C\pi\text{-}H_3O^+ + Cd^{2+} \rightarrow C\pi\text{-}Cd^{2+} + H_3O^+ \quad (23)$$

5. Conclusions

MBC was prepared by modifying a *Pennisetum sp*. straw biochar with $MgCl_2$, and the Cd^{2+} adsorption mechanisms of both the pristine (BC) and modified (MBC) biochars were studied. The maximum theoretical adsorption capacity of Cd^{2+} on MBC was 763.12 mg/g, and the adsorption data of MBC fitted the Langmuir isotherm and pseudo-second order kinetic models. After the adsorption of Cd^{2+}, a precipitation of $Cd(OH)_2$ on MBC surfaces, and formation of --COO-Cd and -O-Cd complexes releasing Mg^{2+}, Ca^{2+} and K^+ into the solution, were observed. Moreover, aromatic structures of the biochar (≥ 500 °C) surface acted as π donors during the Cd^{2+} adsorption process. The contribution of Cd^{2+} adsorption mechanisms on MBC was in the order of Q_{cmp} (73.43%) > Q_{cme} (22.67%) > $Q_{c\pi}$ (3.88%). The results suggested that $MgCl_2$-modified biochar has a good potential for Cd^{2+} removal from contaminated

water. This paper thus shows the possibility of preparing a highly efficient Cd^{2+}-adsorbing material via engineering biochar surfaces with $MgCl_2$, encouraging the development of novel biochar materials via simple and eco-friendly methods.

CRediT authorship contribution statement

Guangcai Yin: Conceptualization, Investigation, Methodology, Writing - original draft. **Lin Tao:** Investigation, Methodology, Writing - original draft. **Xinglin Chen:** Investigation, Methodology. **Nanthi S. Bolan:** Writing - review & editing. **Binoy Sarkar:** Result interpretation; Writing - review & editing. **Qintie Lin:** Methodology. **Hailong Wang:** Conceptualization, Supervision, Writing - review & editing.

Declaration of Competing Interest

The authors declare that they have no competing financial interests or personal relationship that could have appeared to influence the work reported in this paper.

Acknowledgements

This work was financially supported by the National Key Research and Development Program of China (2018YFC1800304, 2018YFC1802803), Science and Technology Project of Guangzhou City, China (202103000018), Natural Science and Technology Project of Guangdong Province, China (2016A030313697), and Special Fund for the Science and Technology Innovation Team of Foshan, China (1920001000083).

References

Bandara, T., Franks, A., Xu, J., Bolan, N., Wang, H., Tang, C., 2019. Chemical and biological immobilization mechanisms of potentially toxic elements in biochar-amended soils. Crit. Rev. Environ. Sci. Technol. 50(9), 903-978.

Cao, X., Lena, M., Bin, G., Willie, H., 2009. Dairy-manure derived biochar effectively sorbs lead and atrazine. Environ. Sci. Technol. 43, 3285-3291.

Chang, R., Sohi, S.P., Jing, F., Liu, Y., Chen, J., 2019. A comparative study on biochar properties and Cd adsorption behavior under effects of ageing processes of leaching, acidification and oxidation. Environ. Pollut. 254(Pt B), 113123.

Chen, H., Yang, X., Wang, H., Sarkar, B., Shaheen, S.M., Gielen, G., Bolan, N., Guo, J., Che, L., Sun, H., Rinklebe, J., 2020. Animal carcass- and wood-derived biochars improved nutrient bioavailability, enzyme activity, and plant growth in metal-phthalic acid ester co-contaminated soils: A trial for reclamation and improvement of degraded soils. J. Environ. Manag. 261, 110246.

Chen, Q., Qin, J., Cheng, Z., Huang, L., Sun, P., Chen, L., Shen, G., 2018. Synthesis of a stable magnesium-impregnated biochar and its reduction of phosphorus leaching from soil. Chemosphere. 199, 402-408.

Chen, Y., Shan, R., Sun, X., 2020. Adsorption of cadmium by magnesium-modified biochar at different pyrolysis temperatures. Bioresources. 15(1), 767-786.

Cui, X., Fang, S., Yao, Y., Li, T., Ni, Q., Yang, X., He, Z., 2016. Potential mechanisms of cadmium removal from aqueous solution by Canna indica derived biochar. Sci. Total Environ. 562, 517-525.

Deng, Y., Huang, S., Laird, D.A., Wang, X., Dong, C., 2018. Quantitative mechanisms of cadmium adsorption on rice straw- and swine manure-derived biochars. Environ. Sci. Pollut. Res. Int. 25(32), 32418-32432.

Ennis, C.J., Evans, A.G., Islam, M., Ralebitso Senior, T.K., Senior, E., 2012. Biochar: Carbon sequestration, land remediation, and impacts on soil microbiology. Crit. Rev. Environ. Sci.Technol. 42(22), 2311-2364.

Harvey, O.R., Herbert, B.E., Rhue, R.D., Kuo, L., 2011. Metal interactions at the biochar-water interface: energetics and structure-sorption relationships elucidated by flow adsorption microcalorimetry. Environ. Sci. Technol. 45(13), 5550-5556.

Hong, J., Xie, J., Mirshahghassemi, S., Lead, J., 2020. Metal (Cd, Cr, Ni, Pb) removal from environmentally relevant waters using polyvinylpyrrolidone-coated magnetite nanoparticles. RSC Adv. 10(6), 3266-3276.

Hou, J. 2017. Study on the performance and mechanism of phosphorus adsorption by cow dung biochar modified with magnesium on farmland soil. Kunming University of Science and Technology.

Ho, Y.S., McKay, G., 1998. A comparison of chemisorption kinetic models applied to pollutant removal on various sorbents. Process Saf. Environ. Prot. 76(4), 332-340.

Jin, Z., Jia, Y., Zhang, K., Kong, L., Sun, B., Shen, W., Meng, F., Liu, J., 2016. Effective removal of fluoride by porous MgO nanoplates and its adsorption mechanism. J. Alloy Comp. 675, 292-300.

Khan, Z.H., Gao, M., Qiu, W., Islam, M.S., Song, Z., 2020. Mechanisms for cadmium adsorption by magnetic biochar composites in an aqueous solution. Chemosphere. 246, 125701.

Kim, D.W., Wee, J.H., Yang, C.M., Yang, K.S., 2020. Efficient removals of Hg and Cd in aqueous solution through NaOH-modified activated carbon fiber. Chem. Eng. J. 392, 123768.

Kuang, M., Shang, Y., Yang, G., Liu, B., Yang, B., 2019. Facile synthesis of hollow mesoporous MgO spheres via spray-drying with improved adsorption capacity for Pb(II) and Cd(II). Environ. Sci. Pollut. Res. 26(18), 18825-18833.

Kwon, G., Bhatnagar, A., Wang, H., Kwon, E.E., Song, H., 2020. A review of recent advancements in utilization of biomass and industrial wastes into engineered biochar. J. Hazard. Mater. 400, 123242.

Li, A., Deng, H., Jiang, Y., Ye, C., Yu, B., Zhou, X., Ma, A., 2020. Superefficient removal of heavy metals from wastewater by Mg-loaded biochars: Adsorption characteristics and removal mechanisms. Langmuir. 36(31), 9160-9174.

Li, B., Yang, L., Wang, C., Zhang, Q., Liu, Q., Li, Y., Xiao, R., 2017. Adsorption of Cd(II) from aqueous solutions by rape straw biochar derived from different modification processes. Chemosphere. 175, 332-340.

Li, R., Wang, J., Zhou, B., Awasthi, M.K., Ali, A., Zhang, Z., Lahori, A.H., Mahar, A., 2016. Recovery of phosphate from aqueous solution by magnesium oxide decorated magnetic biochar and its potential as phosphate-based fertilizer substitute. Bioresour. Technol. 215, 209-214.

Li, Y., Shao, J., Wang, X., Deng, Y., Yang, H., Chen, H., 2014. Characterization of modified biochars derived from bamboo pyrolysis and their utilization for target component (furfural) adsorption. Energy Fuel. 28, 5119-5127.

Lian, F., Sun, B., Chen, X., Zhu, L., Liu, Z., Xing, B., 2015. Effect of humic acid (HA) on sulfonamide sorption by biochars. Environ. Pollut. 204, 306-312.

584 Lian, W., Yang, L., Joseph, S., Shi, W., Bian, R., Zheng, J., Li, L., Shan, S., Pan, G., 2020.
585 Utilization of biochar produced from invasive plant species to efficiently adsorb Cd(II) and
586 Pb(II). Bioresour. Technol. 317, 124011.
587 Ling, L., Liu, W., Zhang, S., Jiang, H., 2017. Magnesium oxide embedded nitrogen self-doped
588 biochar composites: Fast and high-efficiency adsorption of heavy metals in an aqueous
589 solution. Environ. Sci. Technol. 51(17), 10081-10089.
590 Liu, K., Li, F., Cui, J., Yang, S., Fang, L., 2020. Simultaneous removal of Cd(II) and As(III) by
591 graphene-like biochar-supported zero-valent iron from irrigation waters under aerobic
592 conditions: Synergistic effects and mechanisms. J. Hazard. Mater. 395, 122623.
593 Liu, W., Jiang, H., Tian, K., Ding, Y., Yu, H., 2013. Mesoporous carbon stabilized MgO
594 nanoparticles synthesized by pyrolysis of $MgCl_2$ preloaded waste biomass for highly
595 efficient CO_2 capture. Environ. Sci. Technol. 47(16), 9397-9403.
596 Lu, H., Zhang, W., Yang, Y., Huang, X., Wang, S., Qiu, R., 2012. Relative distribution of Pb^{2+}
597 sorption mechanisms by sludge-derived biochar. Water Res. 46(3), 854-62.
598 Małgorzata, K.Z., Filipkowska, U., Jóźwiak, T., 2020. Adsorption of Cu(II) and Cd(II) from
599 aqueous solutions by chitosan immobilized in alginate beads. J. Environ. Chem. Eng. 8(4),
600 103878.
601 Mia, S., Dijkstra, F.A., Singh, B., 2017. Aging Induced changes in biochar's functionality and
602 adsorption behavior for phosphate and ammonium. Environ. Sci. Technol. 15(51), 8359-
603 8367.
604 Nie, T., Yang, X., Chen, H., Muller, K., Shaheen, S.M., Rinklebe, J., Song, H., Xu, S., Wu, F.,
605 Wang, H., 2021. Effect of biochar aging and co-existence of diethyl phthalate on the mono-
606 sorption of cadmium and zinc to biochar-treated soils. J. Hazard. Mater. 408, 124850.
607 Purkayastha, D., Mishra, U., Biswas, S., 2014. A comprehensive review on Cd(II) removal from
608 aqueous solution. J. Water Process. Eng. 2, 105-128.
609 Qiu, Y., Zhang, Q., Li, M., Fan, Z., Sang, W., Xie, C., Niu, D., 2019. Adsorption of Cd(II) from
610 aqueous solutions by modified biochars: Comparison of modification methods. Water Air
611 Soil Pollut. 230(4), 84.
612 Sarkar, B., Megharaj, M., Xi, Y., Naidu, R., 2012. Surface charge characteristics of organo-
613 palygorskites and adsorption of p-nitrophenol in flow-through reactor system. Chem. Eng.

614 J. 185-186, 35-43.
615 Shaheen, S.M., Niazi, N.K., Hassan, N.E.E., Bibi, I., Wang, H., Tsang, D.C.W., Ok, Y.S., Bolan,
616 N., Rinklebe, J., 2019. Wood-based biochar for the removal of potentially toxic elements in
617 water and wastewater: a critical review. Inter. Mater. Rev. 64(4), 216-247.
618 Takaya, C.A., Fletcher, L.A., Singh, S., Okwuosa, U.C., Ross, A.B., 2016. Recovery of
619 phosphate with chemically modified biochars. J. Environ. Chem. Eng. 4(1), 1156-1165.
620 Tao, Q., Li, B., Li, Q., Han, X., Jiang, Y., Jupa, R., Wang, C., Li, T., 2019. Simultaneous
621 remediation of sediments contaminated with sulfamethoxazole and cadmium using
622 magnesium-modified biochar derived from Thalia dealbata. Sci. Total Environ. 659, 1448-
623 1456.
624 Tian, G., Wang, W., Zong, L., Wang, A., 2017. MgO/palygorskite adsorbent derived from
625 natural Mg-rich brine and palygorskite for high-efficient removal of Cd(II) and Zn(II) ions.
626 J. Environ. Chem. Eng. 5(1), 1027-1036.
627 Wan, S., Qiu, L., Tang, G., Chen, W., Li, Y., Gao, B., He, F., 2020. Ultrafast sequestration of
628 cadmium and lead from water by manganese oxide supported on a macro-mesoporous
629 biochar. Chem. Eng. J. 387, 124095.
630 Wang, R., Huang, D., Liu, Y., Zhang, C., Lai, C., Zeng, G., Cheng, M., Gong, X., Wan, J., Luo,
631 H., 2018. Investigating the adsorption behavior and the relative distribution of Cd^{2+} sorption
632 mechanisms on biochars by different feedstock. Bioresour. Technol. 261, 265-271.
633 Wei, J., Tu, C., Yuan, G., Bi, D., Xiao, L., Theng, B.K.G., Wang, H., Ok, Y.S., 2019. Carbon-
634 coated montmorillonite nanocomposite for the removal of chromium(VI) from aqueous
635 solutions. J. Hazard. Mater. 368, 541-549.
636 Wen, E., Yang, X., Chen, H., Shaheen, S.M., Sarkar, B., Xu, S., Song, H., Liang, Y., Rinklebe,
637 J., Hou, D., Li, Y., Wu, F., Pohorely, M., Wong, J.W.C., Wang, H., 2021. Iron-modified
638 biochar and water management regime-induced changes in plant growth, enzyme activities,
639 and phytoavailability of arsenic, cadmium and lead in a paddy soil. J. Hazard. Mater. 407,
640 124344.
641 Wu, J., Wang, T., Zhang, Y., Pan, W., 2019. The distribution of Pb(II)/Cd(II) adsorption
642 mechanisms on biochars from aqueous solution: Considering the increased oxygen
643 functional groups by HCl treatment. Bioresour. Technol. 291, 121859.

644 Wu, J., Wang, T., Wang, J., Zhang, Y., Pan, W., 2021. A novel modified method for the efficient
645 removal of Pb and Cd from wastewater by biochar: Enhanced the ion exchange and
646 precipitation capacity. Sci. Total Environ. 754, 142150.
647 Wu, P., Liao, Z., Zhang, H., Guo, J., 2001. Adsorption of phenol on inorganic-organic pillared
648 montmorillonite in polluted water. Environ. Int. 26(5-6), 401-407.
649 Xiang, J., Lin, Q., Cheng, S., Guo, J., Yao, X., Liu, Q., Yin, G., Liu, D., 2018a. Enhanced
650 adsorption of Cd(II) from aqueous solution by a magnesium oxide–rice husk biochar
651 composite. Environ. Sci. Pollut. Res. 25(14), 14032-14042.
652 Xie, M., Chen, W., Xu, Z., Zheng, S., Zhu, D., 2014. Adsorption of sulfonamides to
653 demineralized pine wood biochars prepared under different thermochemical conditions.
654 Environ. Pollut. 186, 187-194.
655 Xiong, C., Wang, W., Tan, F., Luo, F., Chen, J., Qiao, X., 2015. Investigation on the efficiency
656 and mechanism of Cd(II) and Pb(II) removal from aqueous solutions using MgO
657 nanoparticles. J. Hazard. Mater. 299, 664-674.
658 Xiong, L., Chen, C., Chen, Q., Ni, J., 2011. Adsorption of Pb(II) and Cd(II) from aqueous
659 solutions using titanate nanotubes prepared via hydrothermal method. J. Hazard. Mater.189,
660 741-748.
661 Yao, Y., Gao, B., Inyang, M., Zimmerman, A.R., Cao, X., Pullammanappallil, P., Yang, L., 2011.
662 Removal of phosphate from aqueous solution by biochar derived from anaerobically
663 digested sugar beet tailings. J. Hazard. Mater. 190(1-3), 501-507.
664 Yin, G., Bi, L., Song, X., Luo, H., Ji, P., Lin, Q., Liu, Q., Tang, G., 2019. Adsorption of Cd(II)
665 from aqueous solution by *Pennisetum sp*. straw biochars derived from different modification
666 methods. Environ. Sci. Pollut. Res. 26(7), 7024-7032.
667 Yin, G., Song, X., Tao, L., Sarkar, B., Sarmah, A.K., Zhang, W., Lin, Q., Xiao, R., Liu, Q.,
668 Wang, H., 2020. Novel Fe-Mn binary oxide-biochar as an adsorbent for removing Cd(II)
669 from aqueous solutions. Chem. Eng. J. 389, 124465.
670 Yin, Q., Wang, R., Zhao, Z., 2018a. Application of Mg-Al-modified biochar for simultaneous
671 removal of ammonium, nitrate, and phosphate from eutrophic water. J. Clean. Prod. 176,
672 230-240.
673 Yin, Z., Liu, Y., Liu, S., Jiang, L., Tan, X., Zeng, G., Li, M., Liu, S., Tian, S., Fang, Y., 2018b.

674 Activated magnetic biochar by one-step synthesis: Enhanced adsorption and coadsorption
675 for 17β-estradiol and copper. Sci. Total Environ. 639, 1530-1542.
676 Yoon, K., Cho, D.W., Tsang, D.C.W., Bolan, N., Rinklebe, J., Song, H., 2017. Fabrication of
677 engineered biochar from paper mill sludge and its application into removal of arsenic and
678 cadmium in acidic water. Bioresour. Technol. 246, 69-75.
679 Zhang, C., Shan, B., Tang, W., Zhu, Y., 2017a. Comparison of cadmium and lead sorption by
680 Phyllostachys pubescens biochar produced under a low-oxygen pyrolysis atmosphere.
681 Bioresour. Technol. 238, 352-360.
682 Zhang, D., Zhang, K., Hu, X., He, Q., Yan, J., Xue, Y., 2021. Cadmium removal by $MgCl_2$
683 modified biochar derived from crayfish shell waste: Batch adsorption, response surface
684 analysis and fixed bed filtration. J. Hazard. Mater. 408, 124860.
685 Zhang, J., Hu, D., Shen, Z., Jin, F., David, O., Pan, S., Yong, S., Daniel, C., Bolan, N., Daniel,
686 C., 2020. Effects of excessive impregnation, magnesium content, and pyrolysis temperature
687 on MgO-coated watermelon rind biochar and its lead removal capacity solution. Environ.
688 Res. 183, 109152.
689 Zhang, J., Hu, X., Yan, J., Long, L., Xue, Y., 2020a. Crayfish shell biochar modified with
690 magnesium chloride and its effect on lead removal in aqueous solution. Environ. Sci. Pollut.
691 Res. 27(9), 9582-9588.
692 Zhang, J., Ma, X., Yuan, L., Zhou, D., 2020b. Comparison of adsorption behavior studies of
693 Cd^{2+} by vermicompost biochar and $KMnO_4$-modified vermicompost biochar. J. Environ.
694 Manage. 256, 109959.
695 Zhang, M., Gao, B., Yao, Y., Xue, Y., Inyang, M., 2012. Synthesis of porous MgO-biochar
696 nanocomposites for removal of phosphate and nitrate from aqueous solutions. Chem. Eng.
697 J. 210, 26-32.
698 Zhang, S., Zhang, H., Cai, J., Zhang, X., Zhang, J., Shao, J., 2017b. Evaluation and prediction
699 of cadmium removal from aqueous solution by phosphate-modified activated bamboo
700 biochar. Energy Fuel. 32(4), 4469-4477.
701 Zhu, Z., Li, W., 2012. Effect of magnesium oxide on adsorption of Cd^{2+} from aqueous solution.
702 RSC Adv. 2(12), 5178-5184.
703 Zhu S., Zhao J., Zhao N., Yang X., Chen C., Shang J., 2020. Goethite modified biochar as a

multifunctional amendment for cationic Cd(II), anionic As(III), roxarsone, and phosphorus in soil and water. J. Clean. Prod. 247, 119579.

Zong, P., Cheng, Y., Wang, S., Wang, L., 2020. Simultaneous removal of Cd(II) and phenol pollutions through magnetic graphene oxide nanocomposites coated polyaniline using low temperature plasma technique. Int. J. Hydrog. Energy. 45(38), 20106-20119.

Table 1

Physical and chemical properties of the pristine and $MgCl_2$-modified biochars

Biochar	Elemental content (%)					Atomic ratio			pH	Ash %	S_{BET} m^2/g	Pore Volume cm^3/g	Pore diameter nm
	C	H	O	N	S	H/C	O/C	(O+N)/C					
BC	61.85	2.19	33.65	0.21	2.52	0.43	0.41	0.41	10.71	25.44	1.90	0.0042	8.94
MBC	50.22	2.67	44.05	0.24	2.82	0.64	0.66	0.66	10.46	31.67	202.75	0.1689	3.33

Table 2

Kinetic parameters of Cd^{2+} adsorption on BC and MBC fitted to the pseudo-first (PFOM) and pseudo-second (PSOM) order models

Adsorbents	PFOM						PSOM					
	q_e (mg/g)	k_2 (g/(mg·min))	R^2	R^2_{adj}	RMSE	RPD	q_e (mg/g)	k_1 (min^{-1})	R^2	R^2_{adj}	RMSE	RPD
BC	43.2	0.2267	0.9999	0.9999	0.8652	4.75	43.6	0.0096	0.9999	0.9999	0.0828	49.64
MBC	759.5	0.0050	0.9989	0.9988	1.1450	3.90	866.7	8.9230	0.9990	0.9989	0.0483	92.34

Table 3

Isotherm parameters of Cd^{2+} adsorption fitted to the Langmuir and Freundlich models

Adsorbents	Langmuir model						Freundlich model					
	K_L (L/mg)	q_m (mg/g)	R^2	R^2_{adj}	RMSE	RPD	1/n	K_F $((mg/g)(L/mg)^{1/n})$	R^2	R^2_{adj}	RMSE	RPD
BC	0.0927	68.4	0.9940	0.9930	0.0372	52.69	0.1483	30.5	0.9618	0.9557	0.1220	16.07
MBC	2.8115	763.1	0.9809	0.9782	0.0112	314.29	0.2122	211.6	0.9417	0.9333	0.4944	7.12

Table 4

Adsorption capacity and estimated contribution of each adsorption mechanism for Cd^{2+} adsorption by pristine and $MgCl_2$-modified biochars

Adsorbent	Adsorption capacity (mg/g)						Proportion of each mechanism (%)					
	Q_{cmp}	Q_{cme}	$Q_{c\pi}$	Q_p	Q_e	Q_{co}	Q_{cmp}	Q_{cme}	$Q_{c\pi}$	Q_p	Q_e	Q_{co}
BC	38.50	22.90	6.51	0.21	0.26	0.03	56.28	33.47	9.52	0.31	0.38	0.03
MBC	560.38	173.00	29.63	0.04	0.00	0.07	73.43	22.67	3.88	0.00	0.00	0.00

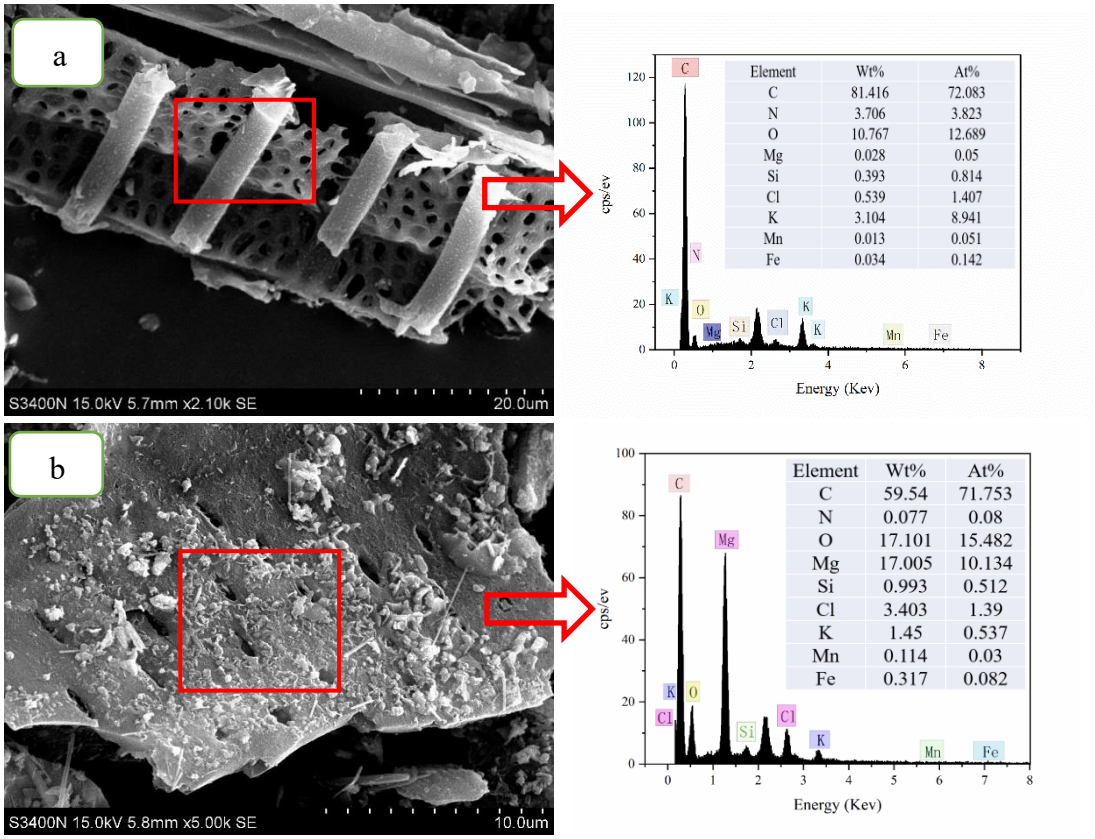

Fig. 1. SEM images (left) and EDX spectra (right) of (a) pristine biochar (BC), and (b) $MgCl_2$-modified biochar (MBC)

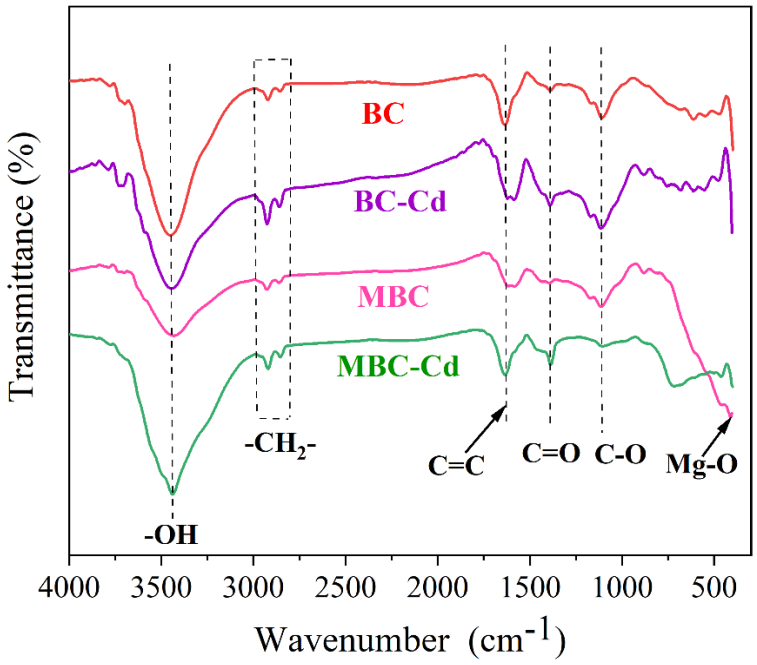

731
732

Fig. 2. FTIR spectra of BC/MBC before and after Cd^{2+} adsorption

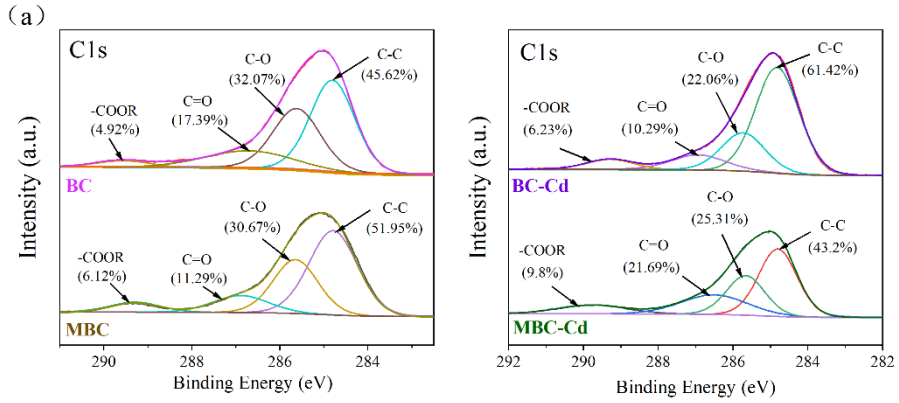

733

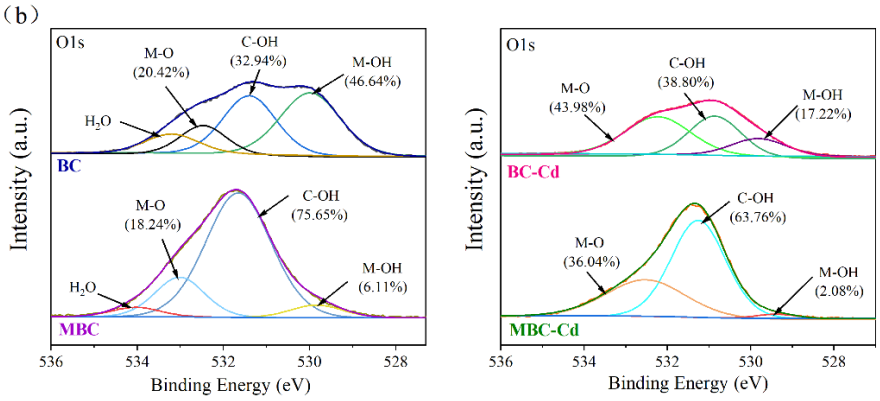
(b)
O1s
M-O
(20.42%)
C-OH
(32.94%)
M-OH
(46.64%)
H2O
BC
M-O
(18.24%)
C-OH
(75.65%)
M-OH
(6.11%)
H2O
MBC
Intensity (a.u.)
536
534
532
530
528
Binding Energy (eV)
O1s
M-O
(43.98%)
C-OH
(38.80%)
M-OH
(17.22%)
BC-Cd
C-OH
(63.76%)
M-O
(36.04%)
M-OH
(2.08%)
MBC-Cd
Intensity (a.u.)
536
534
532
530
528
Binding Energy (eV)

734

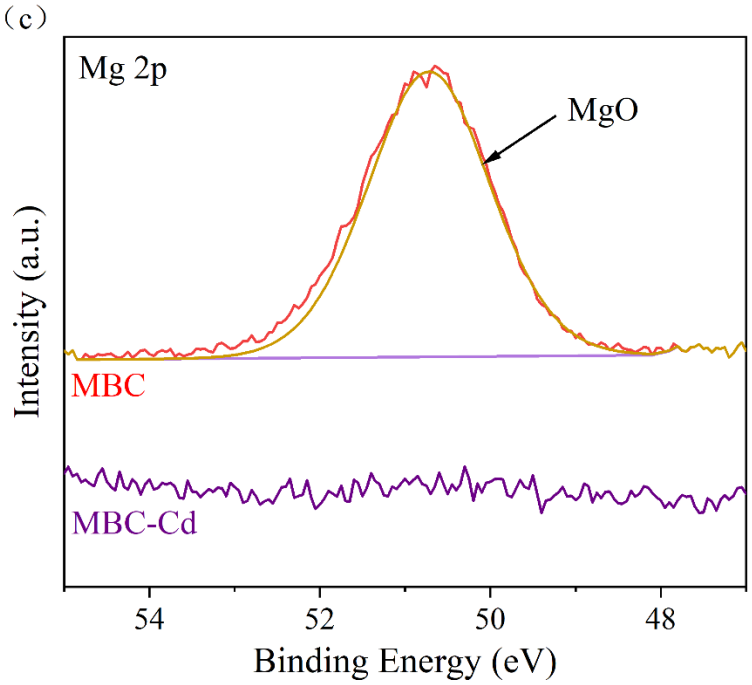
(c)
Mg 2p
MgO
MBC
MBC-Cd
Intensity (a.u.)
54
52
50
48
Binding Energy (eV)

735

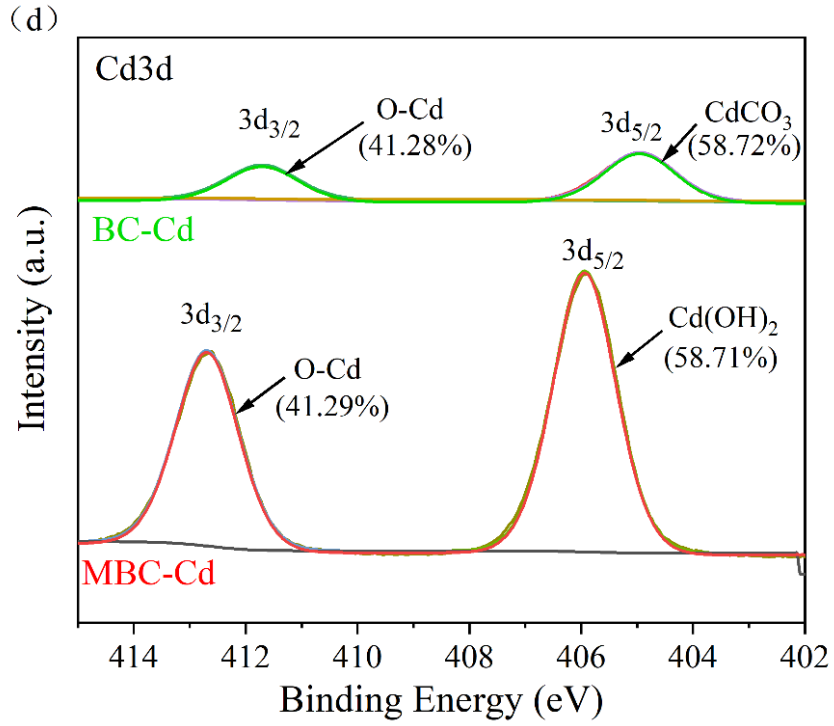

Fig. 3. XPS spectra of BC/MBC for Cd^{2+} adsorption: (a) C1s, (b) O1s, (c) Mg2p, and (d) Cd3d

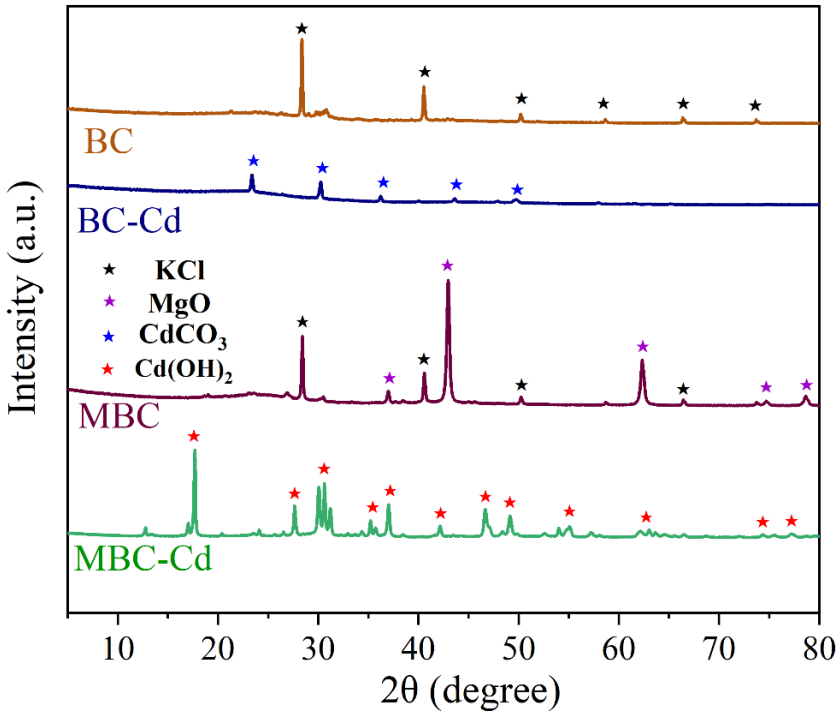

Fig. 4. XRD patterns of BC/MBC before and after Cd^{2+} adsorption

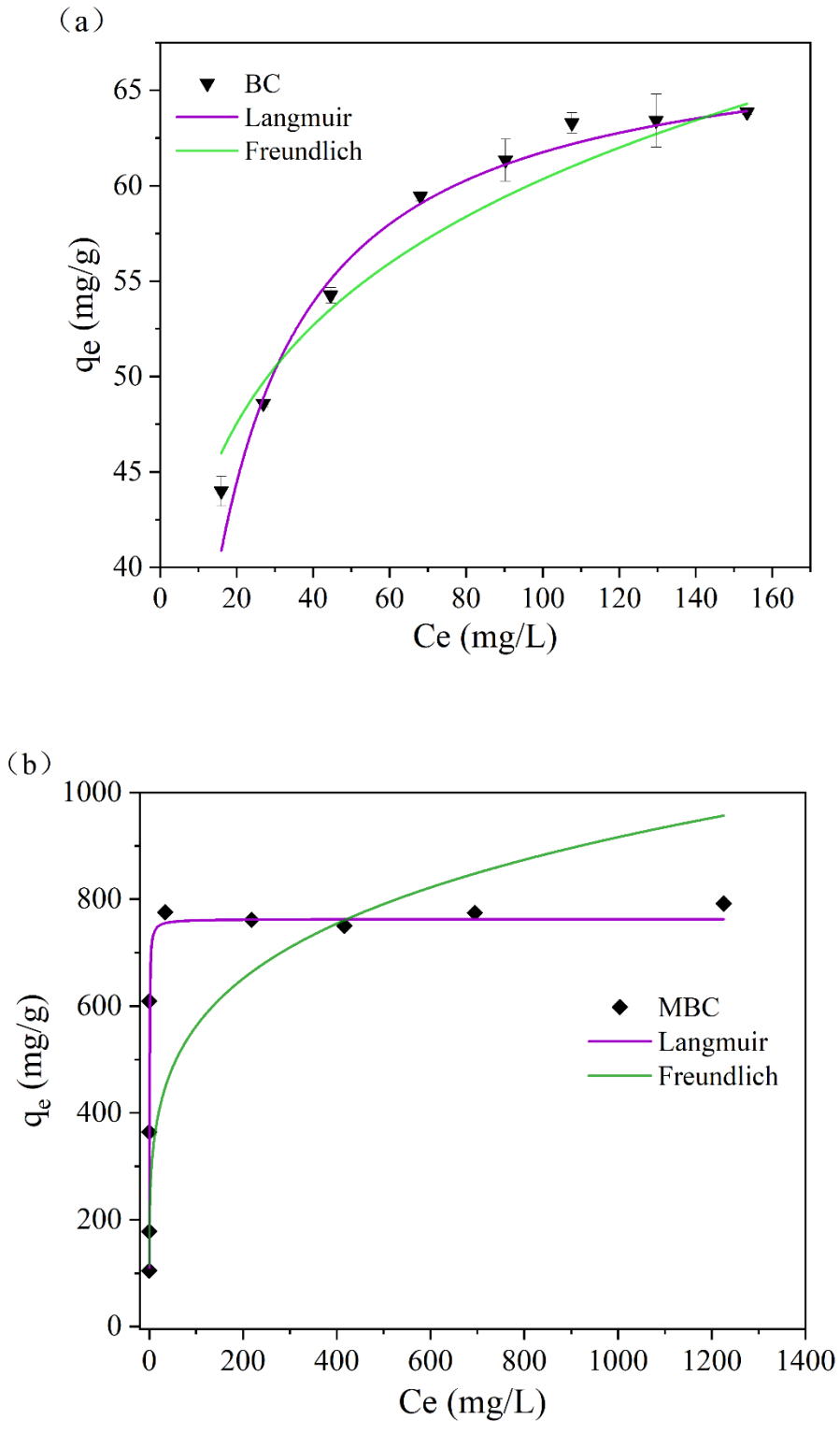

Fig. 5. Fitting of Langmuir and Freundlich isotherm models for the adsorption of Cd^{2+} by (a) BC and (b) MBC

Supplementary Material for:

Quantitative analysis on the mechanism of Cd^{2+} removal by $MgCl_2$-modified biochar in aqueous solutions

Guangcai Yin[a,1], Lin Tao[a,1], Xinglin Chen[a], Nanthi S. Bolan[b], Binoy Sarkar[c], Qintie Lin[a], Hailong Wang[d,e,*]

[a]*Guangdong Industrial Contaminated Site Remediation Technology and Equipment, Engineering Research Center, School of Environmental Science and Engineering, Guangdong University of Technology, Guangzhou, 510006, China*

[b]*The Global Centre for Environmental Remediation, University of Newcastle, Callaghan, NSW, Australia*

[c]*Lancaster Environment Centre, Lancaster University, Lancaster, LA1 4YQ, United Kingdom*

[d] *Biochar Engineering Technology Research Center of Guangdong Province, School of Environmental and Chemical Engineering, Foshan University, Foshan 528000, China*

[e] *Key Laboratory of Soil Contamination Bioremediation of Zhejiang Province, Zhejiang A &F University, Hangzhou 311300, China*

[1] These authors contributed equally to this work and should be considered as co-first authors.

* Correspondence to: School of Environmental and Chemical Engineering, Foshan University, Foshan, Guangdong 528000, China. E-mail address: E-mail address: hailong.wang@fosu.edu.cn (H. Wang).

Table S1

Thermodynamic parameters for the adsorption of Cd^{2+} by biochars

Sample	Temperature (°C)	ΔGº (kJ/mol)	ΔHº (kJ/mol)	ΔSº (J/(mol·K))
BC	25	-8.52	-0.8	25.9
	35	-8.78		
	45	-9.04		
MBC	25	-1.81	8.9	35.93
	35	-2.17		
	45	-2.53		

780 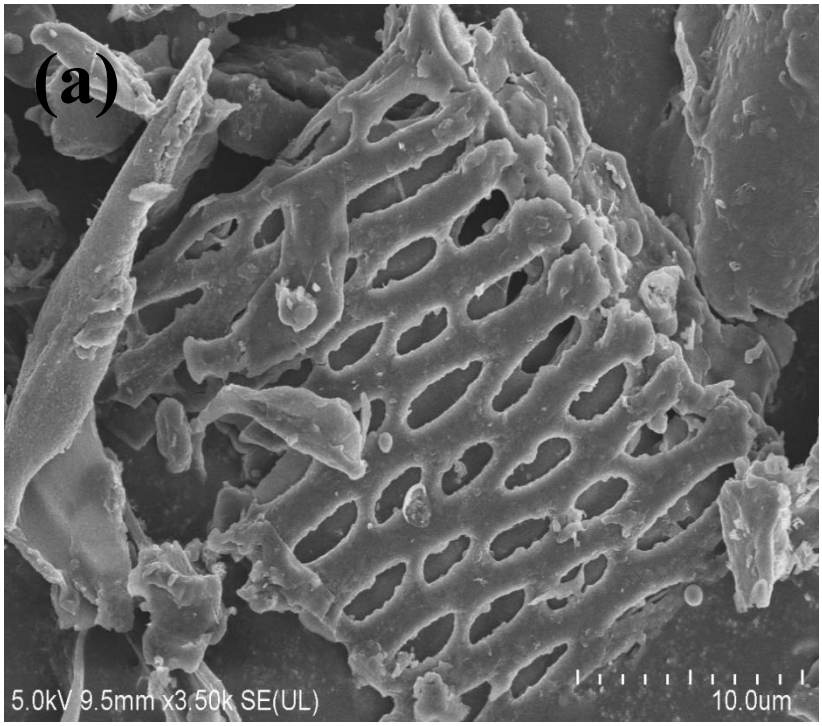

781 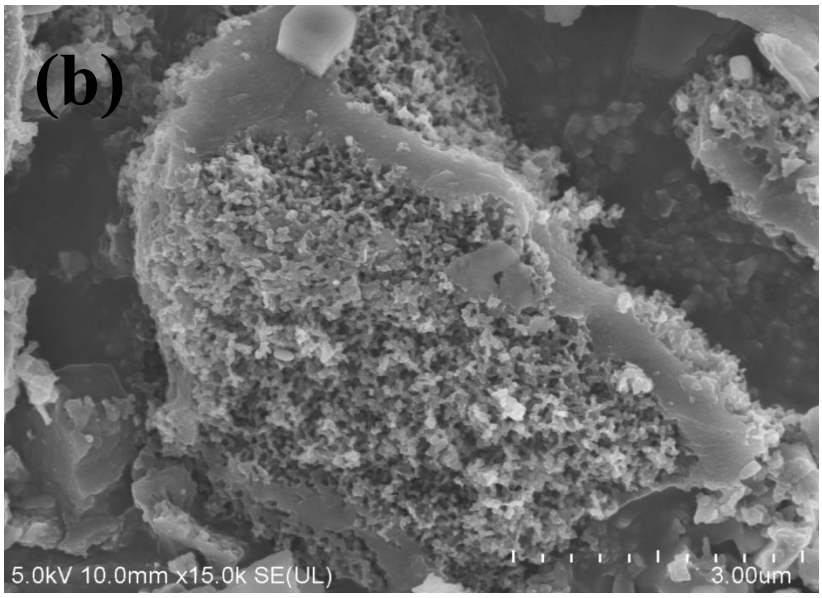

782 **Fig. S1.** SEM images of (a) pristine biochar (BC), and (b) $MgCl_2$-modified biochar
783 (MBC)
784

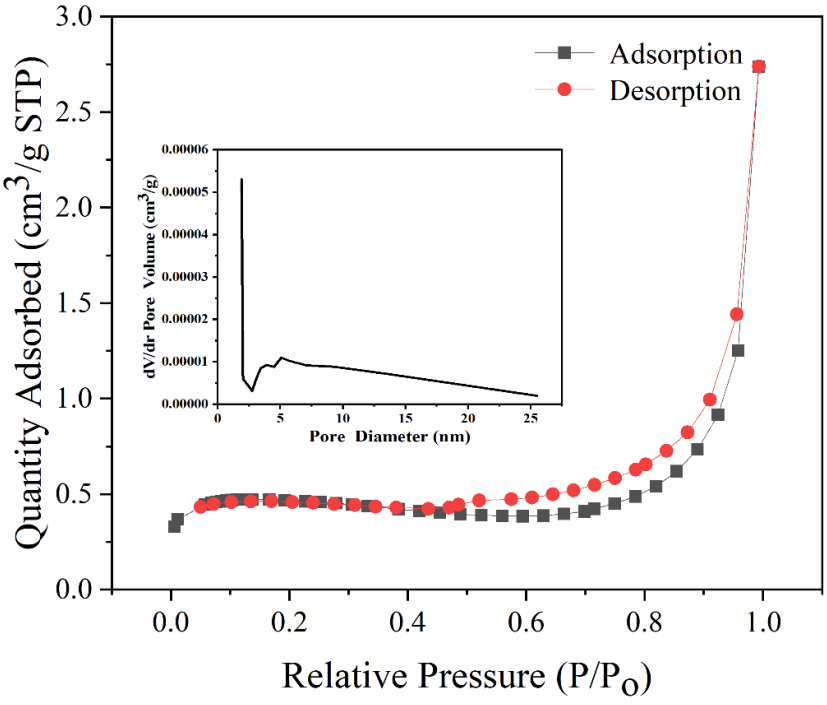

785

786 **Fig.S2**. N_2 adsorption–desorption isotherms of the BC; insetsshow the corresponding
787 pore size distributions

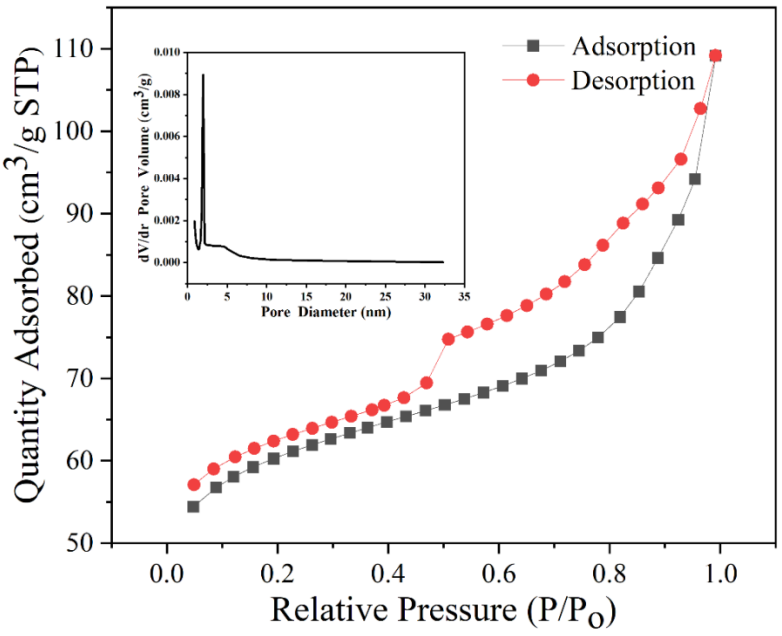

788

789 **Fig. S3**. N_2 adsorption–desorption isotherms of $MgCl_2$-modified biochar; insets show
790 the corresponding pore size distributions

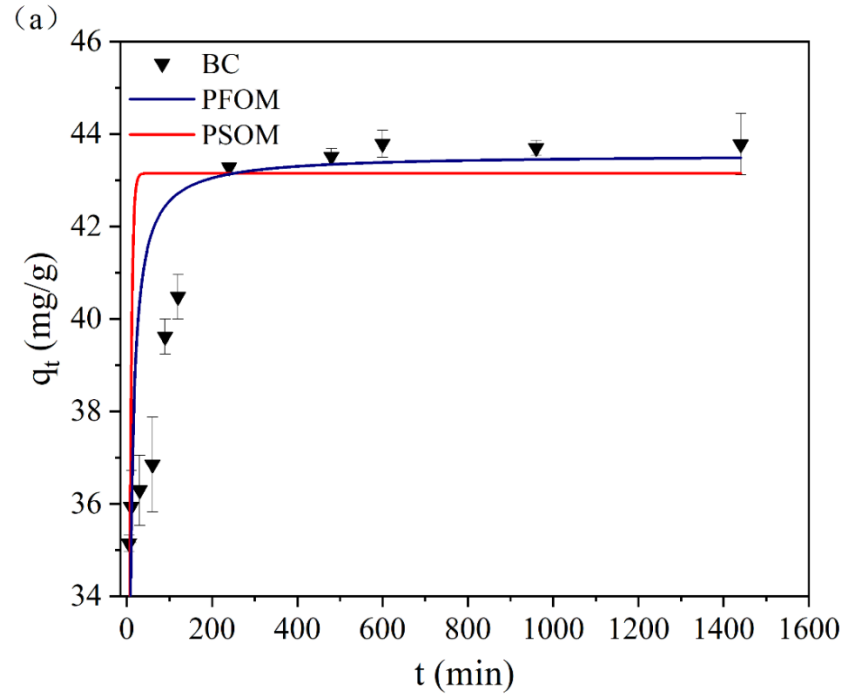

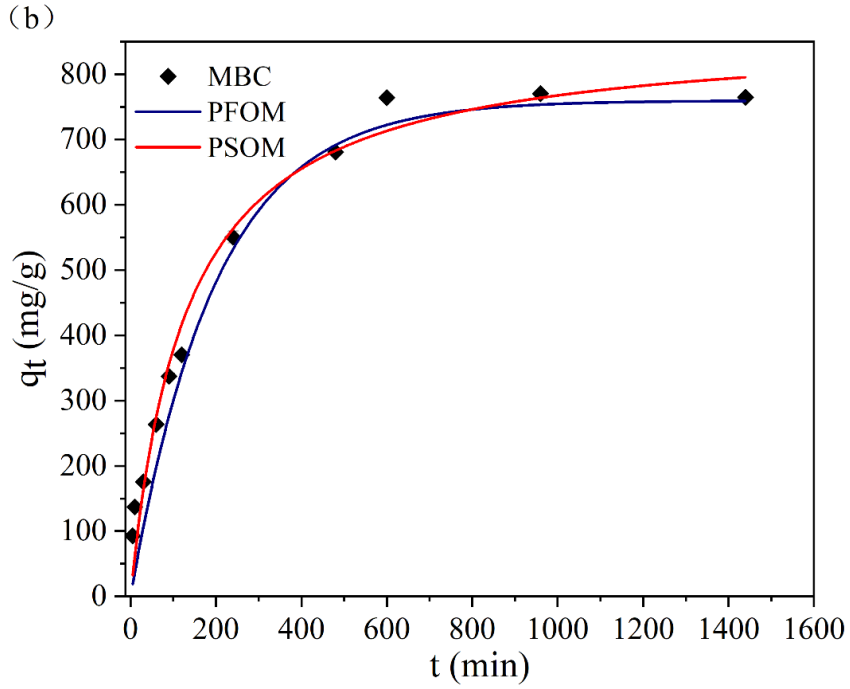

Fig. S4. Fitting of pseudo-first (PFOM) and pseudo-second (PSOM) order kinetic models for the adsorption of Cd^{2+} by (a) BC and (b) MBC

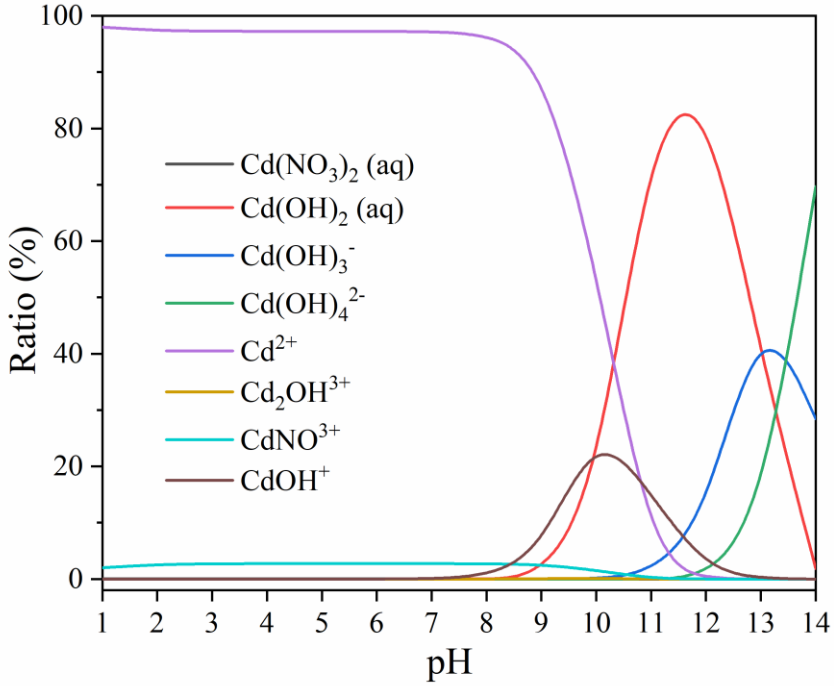

796

797 **Fig. S5.** Distribution of Cd^{2+} species in aqueous solution simulated by Visual
798 MINTEQ

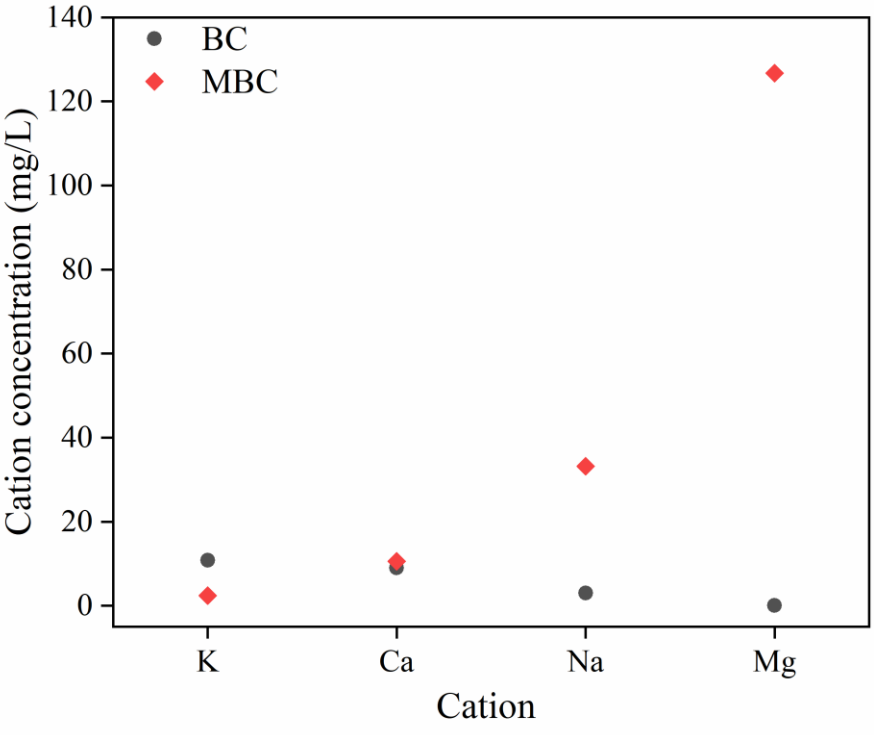

799

800 **Fig. S6.** Net concentrations of Ca^{2+}, Mg^{2+}, K^{+}, and Na^{+} in the solution after Cd^{2+}

adsorption on BC and MBC

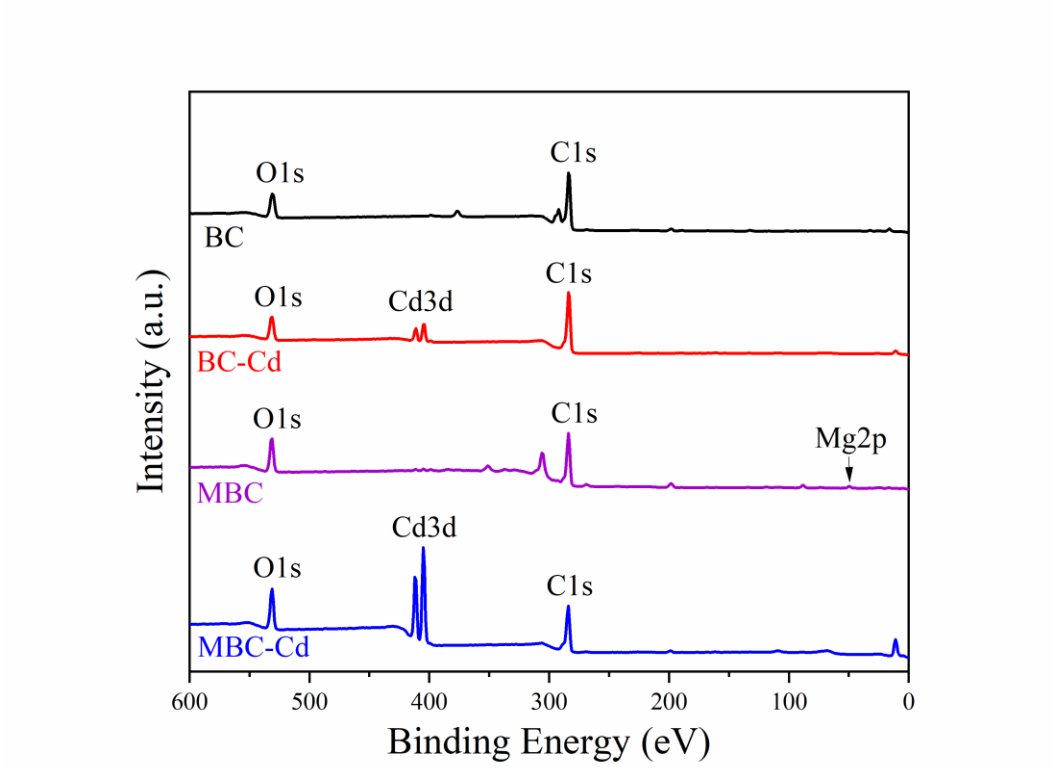

Fig. S7. XPS spectra of BC/MBC before and after Cd^{2+} adsorption